Bull. Chem. Soc. Ethiop. **2025**, 39(6), 1043-1055.
DOI: https://dx.doi.org/10.4314/bcse.v39i6.2

ISSN 1011-3924
Printed in Ethiopia
Online ISSN 1726-801X

THE INFLUENCE OF pH ON THE PROPERTIES OF CHEMICAL BATH DEPOSITED NICKEL SULFIDE FILMS

Ho Soon Min[1*], Adikwu Gowon Jacob[2] and K. Mohanraj[3]

[1]Faculty of Health and Life Sciences, INTI International University, Putra Nilai, 71800, Negeri Sembilan, Malaysia
[2]Department of Industrial Chemistry, Faculty of Physical Sciences, Federal University Dutsin-Ma, P.M.B. 5001, Dutsin-Ma, Katsina State, Nigeria
[3]Department of Physics, Central University of Tamil Nadu, Thiruvarur, 610 005, India

(Received December 6, 2024; Revised February 27, 2025; Accepted March 14, 2025)

ABSTRACT. Nickel sulfide thin films have been prepared on a microscope glass substrate through the chemical bath deposition technique. In this study, nickel sulfate and sodium thiosulfate were utilized to supply nickel ions and sulfide ions, respectively. The surface characteristics of the prepared films were studied with atomic force microscopy. For the first time, X-ray photoelectron spectroscopy and Raman spectroscopy are used to investigate structural information, electronic states and the chemistry of material surfaces. The films produced at pH 4 and pH 5 (acidic environment) are smooth and devoid of cracks, displaying consistent morphology and uniform surface as indicated by atomic force microscopy findings. These properties might improve the efficiency of solar cells when compared to samples made with different pH values.

KEY WORDS: Photovoltaic, Renewable energy, Energy efficiency, Thin films, Nickel sulfide

INTRODUCTION

In the last few decades, several types of chalcogenide-based compounds have been developed for the photovoltaic industry [1], optoelectronic devices [2-4], solar selective coatings [5], sensor devices [6] and laser devices. These films could be produced through chemical bath deposition, metal organic chemical vapor deposition [7], thermal evaporation [8], successive ionic layer adsorption and reaction [9], electro deposition method, sputter deposition, atomic layer deposition [10], close spaced sublimation, sol gel method [11] and plasma enhanced chemical vapor deposition. Among these deposition techniques, chemical bath deposition (CBD) is an inexpensive method, simple to set-up, and produce films onto various types of substrates under lower temperature. Hence, this method was chosen for this study from the perspective of cost-effectiveness and sustainability.

Atomic force microscopy (AFM) is suggested as a powerful measurement tool for determining the topography properties of samples in the field of nanotechnology. It offers several benefits such as non-conductive samples, the ability to magnify in x,y and z axes, and can operate either in air or liquid conditions. AFM was able to capture 3-dimensional images [12] at high resolution (up to atomic level). The operation of this tool was based on the principle of sensing the forces between surface sample and sharp tip. These forces could be either attractive or repulsive, and strongly dependent on the operating modes (Table 1). In contact mode, the AFM probe tip is in contact with the sample surface with high resolution. The forces between the AFM tip and the surface are repulsive. Several advantages have been pointed out such as high scanning speed and the ability scan rougher samples easily. In non-contact mode, the AFM tip is oscillating and eventually, we can see that it never touches the sample. The benefit was this mode can provide the lowest interaction between the sample surface and tip. In tapping mode, the AFM tip oscillates

*Corresponding authors. E-mail: soonmin.ho@newinti.edu.my

and taps the surface of the samples. The advantages included higher lateral resolution, almost no lateral forces, lower forces and less damage. In general, excellent imaging performance strongly depends on the suitable operation mode. It is worth noting that tapping mode could be used in biomedical applications due to these samples are soft and easily ruptured [13]. Contact mode should be avoided because it can deform the biomedical samples during the scanning process. Conventional AFM imaging will take several times to produce a single image and is identified as a time-consuming process. Biomedical samples need imaging at higher frame rates due to the biological process could happen very fast (within milliseconds). High-bandwidth scanner has been developed to enhance the imaging speed. Better performance will be achieved after optimizing imaging parameters including line speed, frame rate, spatial resolution, range and pixel resolution. Other reports have demonstrated that the AFM method (via both tapping and contact mode) could be used to study scaffold design in the bio-sensing and tissue engineering field.

Table 1. Comparison of various types of AFM modes.

	Tapping mode	Contact mode	Non-contact mode
Contact with sample surface	Periodical	Yes	No
Tip loading force	Low	Low to higher	Low
Contamination of AFM tip	Yes	Yes	No
Manipulation of sample	Yes	Yes	No

Raman spectroscopy and X-ray photoelectron spectroscopy (XPS) are very powerful tools used to study the properties of prepared thin films. Chemical and structural information, electronic state, and material surface chemistry are normally investigated using these tools. Raman is defined as a light scattering method [14]. Generally, we can see a lot of peaks in Raman spectrum, representing the wavelength position and intensity of the Raman scattered light. Researchers have explained that each peak accounted for specific groups and individual bonds.

X-ray photoelectron spectroscopy is described as surface-sensitive spectroscopic method and could detect the elements in the prepared materials according to the photoelectric effect. Generally, chemical composition could be identified through the peak position in the x-axis and referred to as binding energy (eV). The binding energy is defined as how much energy is needed to remove electrons from the subshell [15]. We can see that the binding energy is low especially for higher orbitals. Because less energy is needed to eject them when electron is in orbital farther from the nucleus. On the other hand, peak intensity in the y-axis reflected the relative number of electrons that could be observed in the subshell. Typically, peak intensity shows the total number of photoelectrons counts per second. Based on the literature review, these techniques have been used to study different types of nanostructured films such as zinc oxide, copper indium diselenide, copper(II) oxide, Ga_2O_3, tin(II) oxide, manganese(II) oxide, copper indium disulfide, copper indium gallium selenide, and copper indium ditelluride films.

Nickel sulfide (NiS) films are produced on fluorine doped SnO_2 glass using a straightforward electrodeposition technique [16]. Varying the quantities of ammonia added to the deposition solution can greatly affect the morphology of NiS films. The surface structure of NiS counter electrodes transitioned from a network like configuration to nanoparticles when ammonia was present in the deposition bath. Cyclic voltammetry, electrochemical impedance spectroscopy and Tafel tests reveal that the NiS films exhibit excellent conductivity and electrocatalytic characteristics. The power conversion efficiency of dye sensitized solar cells featuring a NiS counter electrode can reach notable levels around 9.65%. Nickel sulfide coated on the surfaces of Fe_2O_3 nanotubes (NiS/Fe_2O_3) through a successive ionic layer adsorption and reaction (SILAR) technique was used as an innovative photoanode in photocathodic protection to slow down the corrosion of 403 stainless steel [17]. The number of SILAR cycles influenced the morphology, visible light response, and associated photoelectrochemical performances of NiS/Fe_2O_3. The results obtained indicated that NiS/Fe_2O_3 prepared with 5 SILAR cycles demonstrated optimal

photoelectrochemical characteristics. The innovative NiS/Fe_2O_3 films used as photoanodes demonstrated an enhanced photocathodic protection effect, leading to 1 200 mV reduction in the potential of the coupled stainless steel in 1 3.5% NaCl solution compared to its corrosion potential. The complexes served as single source precursors for the deposition of nickel sulfide thin films via aerosol assisted chemical vapor deposition [18] at temperatures ranging from 320 to 480 °C. The orthorhombic Ni7S6 was detected at all temperatures, exhibiting spherical tipped wire like crystallite and plates. The orthorhombic Ni9S8 exhibiting flower-like forms was observed at 320 and 360 °C, while branched structures appeared at 400 °C. EDX analysis validated the composition of films produced from all these complexes.

In this work, binary compounds namely nickel sulfide films were prepared on microscope glass slide through chemical bath deposition (CBD) method using nickel sulfate and sodium thiosulfate. Nickel sulfide films are considered as absorber materials in solar cell applications due to crack-free deposition, and uniform morphology. In addition, good coverage contributes to better performance and energy efficiency of solar cells. In general, sunlight can be converted into electricity through solar cells and is said to be one of the popular renewable energy technologies. The influence of pH on the properties of thin films was studied through various techniques. Topography properties were studied using atomic force microscopy (AFM) technique. X-ray photoelectron spectroscopy (XPS) and Raman spectroscopy techniques were employed for investigating the chemical and structural information, electronic state, and material surface chemistry for the first time.

EXPERIMENTAL

In this work, nickel(II) sulfate with a purity of 99.9% (Sigma Aldrich), sodium thiosulfate with a purity of 99.5% (ACS reagent, Sigma Aldrich), hydrochloric acid with a purity of 37% (Thermo Fisher Scientific), and sodium hydroxide with a purity of 98% (Sigma Aldrich) were used. The microscope glass was chosen as substrate for the formation of films. Firstly, glass substrate was cleaned using alcohol for 15 min, followed by distilled water. During the experiment, 0.15 M of nickel sulfate and 0.15 M of sodium thiosulfate were employed as the source of nickel ions and sulfide ions, respectively. The influence of pH value on the properties of the prepared films was studied. Therefore, hydrochloric acid was added drop wise under continuous stirring to reach desired pH value. Finally, the cleaned substrate was vertically immersed into a chemical bath at temperature of 23 °C for 4 hours.

The atomic force microscopy was used for the surface morphology imaging of the obtained samples in a contact mode. The model's name and manufacturer of the AFM used are known as NX-10 and Park system, respectively. X-ray photoelectron spectroscopy spectra were collected on K-Alpha (Model name-Axis Ultra DLD, Manufacturer name: Kratos Analytical) with monochromatic X-ray Al K-alpha radiation at pressure 10^{-9} Torr, was used to investigate elemental composition and electronic states of the nickel sulfide layer. Raman analysis was employed on Raman microscope model LabRam HR evolution (Horiba) under the laser excitation of 325 nm (helium cadmium).

RESULTS AND DISCUSSION

Chemical bath deposition method has been chosen for the preparation of thin films. This method offered many advantages such as simplicity [19], inexpensive technique [20], and formation of materials at lower bath temperature [21, 22]. According to the literature review, nickel nitrate and urea were used to provide nickel ions and sulfide ions, respective during the formation of nanostructured films. In this work, properties of the prepared films (using sodium thiosulfate and nickel sulfate) were studied using Raman Spectroscopy and XPS technique for the first time.

Based on visual observations, the color of mixture has been changed from green to pale green when the pH was reduced from pH 5 to pH 2.2. In addition, sudden sulfur smell was observed at

pH 1. The smell can be explained as the reaction of sodium thiosulfate ($Na_2S_2O_3$) with hydrochloric acid (HCl) to produce sulfur and sulfur dioxide (SO_2). Moreover, a cloudy suspension appeared due to the formation of elemental sulfur which is insoluble in water.

As shown in AFM images (Figure 1), it is noticed that the film coverage was found to increase when the pH value was increased from pH 1 to pH 3.6. Therefore, several defects and pinholes were detected in the thin films prepared at pH 1 to pH 3.6. Conversely, there is a uniform morphology with good coverage for the films prepared at pH 4 and pH 5. These films were appropriate for solar cell applications due to their crack-free morphology [23]. It was noted that well adherent films could be observed onto substrate in these experimental conditions. Based on Sartale and Lokhande report [24], deposition conditions must be optimized to produce well adherent and good quality films onto different substrates such as fluorine doped tin oxide (FTO) coated glass, glass, single crystalline Si(111) wafer substrates.

FTO glass is a see-through conductive metal oxide applicable in creating transparent electrodes for thin film photovoltaics, including organic photovoltaics, amorphous silicon, cadmium telluride, dye sensitized solar cells and hybrid perovskites. FTO glass is also utilized in a diverse array of applications, such as touch screen panels, electromagnetic interference/radio frequency interference shielding, heated glass, anti-static coatings, and light emitting diodes. FTO glass possesses multiple characteristics that render it ideal for manufacturing various optoelectronic devices. These features consist of low surface resistivity, excellent optical transmittance, resistance to scratches and abrasions, thermal stability at elevated temperatures, and inertness to numerous chemicals.

Tun and co-workers [25] have pointed out that good coverage contributes to better performance of solar cells. The morphology of the obtained samples will become a crucial factor in the transportation of holes and electrons. When the films were prepared at pH 5, an irregular distribution of the grain was observed with a large majority of grains being small.

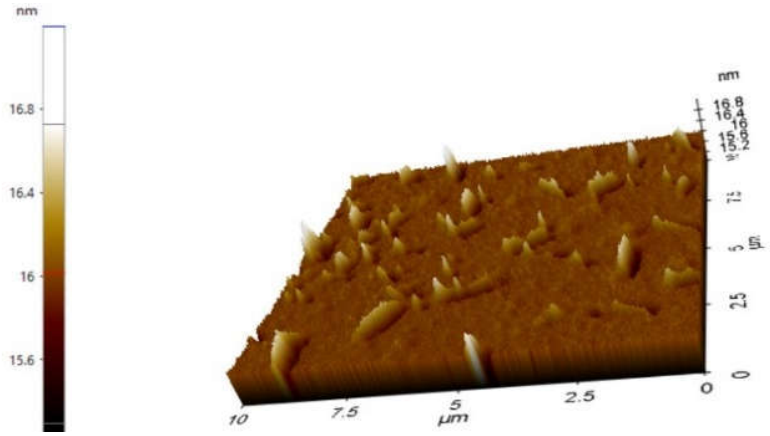

[a]

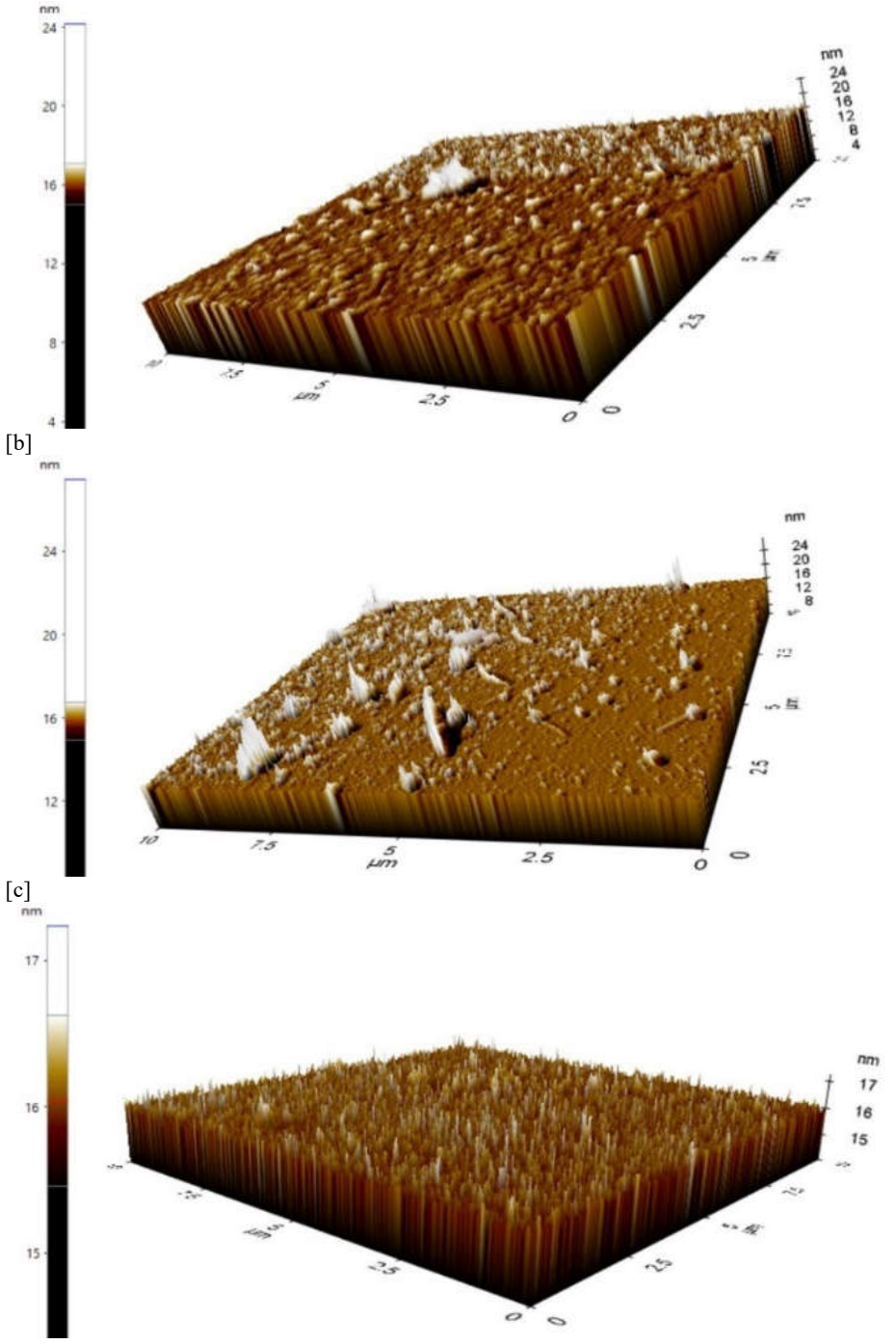
nm
24
20
16
12
8
4
10
7.5
5
µm
2.5
0
[b]
nm
24
20
16
12
10
7.5
5
µm
2.5
0
[c]
nm
17
16
15
2.5
0

[d]

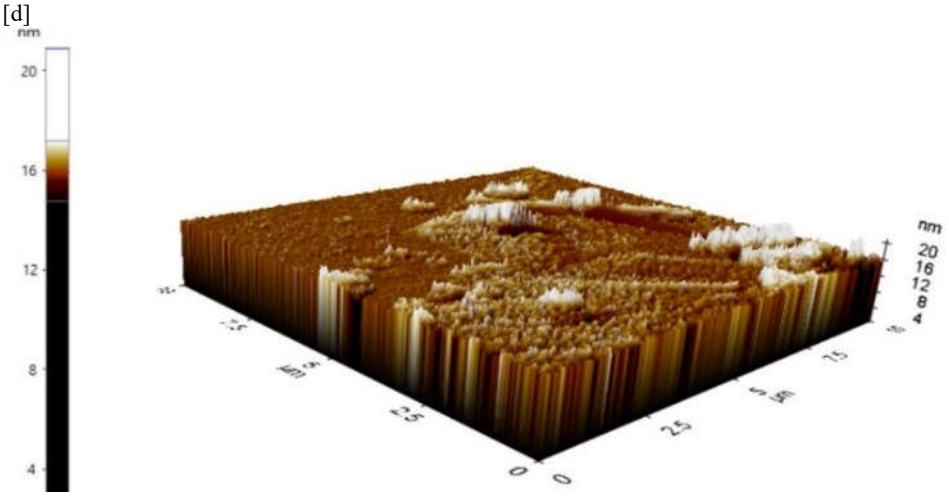

[e]

Figure 1. AFM images of nickel sulfide thin films, prepared under different pH values [a] pH 1, [b] pH 2.2, [c] pH 3.6 , [d] pH 4, and [e] pH 5.

Spray pyrolysis is a method utilized to produce thin films of substances by atomizing a solution with the target material onto a heated surface, where the solvent evaporates, resulting in a solid layer of the desired compound [26]. It is a method in which a liquid precursor is atomized onto a heated surface, resulting in its decomposition and the formation of a thin film on the substrate [27], commonly utilized for creating metal chalcogenide for use such as solar cells and transparent conductive coatings [28].

On the other hand, morphological properties of thin films prepared through spray pyrolysis method have been investigated using scanning electron microscopy technique [29]. It is noted that nano-sheet-like structure (without holes) was observed clearly and can promote the transmission of electrons easily. Proper growth of Ni_7S_6 films (prepared using solvo-thermal technique) was demonstrated by Rekha and co-workers [30]. Based on the field emission scanning electron microscopy, these samples showed rougher surface, offered more electro-catalytic areas for redox process. In addition, they also explain that bigger pore size could be found, resulting in porous structure being developed, which improved Li-ion battery and super capacitor performance. Ni_3S_4 films were synthesized via a simple one-pot hydrothermal method using nickel nitrate and thiourea, as highlighted by Muthu and Gopalan [31]. FESEM studies confirmed flaky structure in the prepared samples, and these flakes were found to be dispersed diversely. In addition, it is noticed that the formation of pores could be seen, enhanced specific surface area. According to obtained results, when the pH was increased from pH 2.2 (thickness = 24 nm), pH 3.6 (thickness = 24 nm) to pH 4 (thickness = 17 nm), the amount of nickel ions will be reduced, but the concentration of hydroxide will increase, leading to reduction in film thickness. These properties were consistent with earlier reports by Arulkumar and co-workers [32], and Kariper and co-workers [33].

Surface roughness of films prepared using different pH values is reported in Table 2. It is noted that the films prepared at pH 3.6 were clearly rougher if compared to other pH values. According to experimental findings, researchers have summarized that the surface roughness was strongly affected by the grain size. Obviously, the surface of the substrates has been occupied by several bigger grains. Technically speaking, rougher surface could be observed when the grain

size was increased. Larger grain samples are inherently rougher because of the increased differences in height. Balayeva and co-workers [34] have observed that bigger grains could be identified in specific experimental conditions (nanostructured films were prepared using SILAR technique), because of coalescing of smaller particles to reduce the Gibb free energy.

Table 2. Surface roughness of the obtained films.

pH value	Sp (maximum peak height)
pH 1	0.0172 μm
pH 2.2	0.0242 μm
pH 3.6	0.0275 μm
pH 4	0.0172 μm
pH 5	0.0209 μm

Figure 2 shows the XPS survey spectra of nickel sulfide (NiS) thin films synthesized at pH 1-5. For all pH examined, the binding energy peaks of the Ni2p and S2p orbits all fall within the ranges of 852-856 eV and 160-164 eV reported in literature [35, 36]. These binding energy ranges suggest the presence of nickel is in a +2, oxidation state and sulfur in a -2, oxidation state, which is consistent with NiS_x (e.g., NiS, Ni_3S_2, NiS_2). The two peak ranges can also indicate the presence of Ni-O bonds (852-856 eV), and S-O bonds (160-164 eV) but more characteristic of Ni-S bonds.

The spectrum of NiS synthesized at pH 1 (Figure 2a) shows the intensity of S2p peak is higher than Ni2p, which implies a sulfide-rich surface. However, for applications in batteries, capacitors and resistors, a nickel-rich surface is required to facilitate electrochemical reactions [37]. By having a surface enriched with nickel ions, the NiS film can facilitate more efficient electrochemical reactions, leading to enhanced battery performance and longevity. Although a high intensity peak of Ni2p at pH 2.2 is observed (Figure 2b), the peak of C1s is at maximum signifying high impurity at the surface. Conversely, at pH 3.6, the binding energy peaks of both Ni2p and S2p have low intensities, which implies that the presence of the Ni^{2+} and S^{2-} ions in the NiS thin film were very minimal.

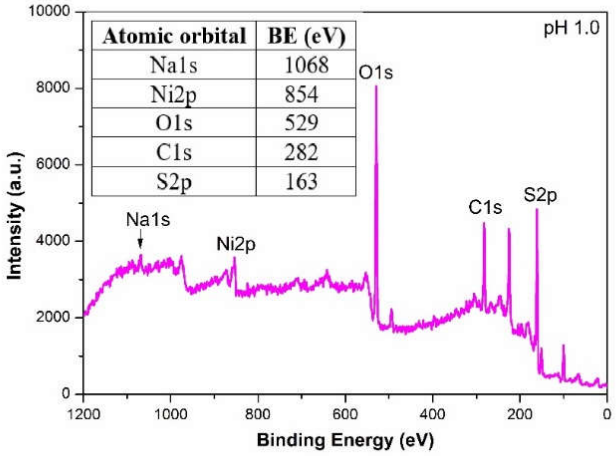

(a)

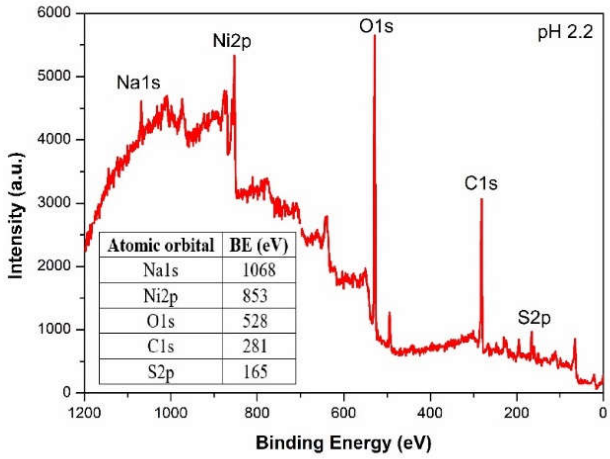
pH 2.2
Ni2p
O1s
Na1s
C1s
S2p
Intensity (a.u.)
Binding Energy (eV)
Atomic orbital | BE (eV)
Na1s | 1068
Ni2p | 853
O1s | 528
C1s | 281
S2p | 165

(b)

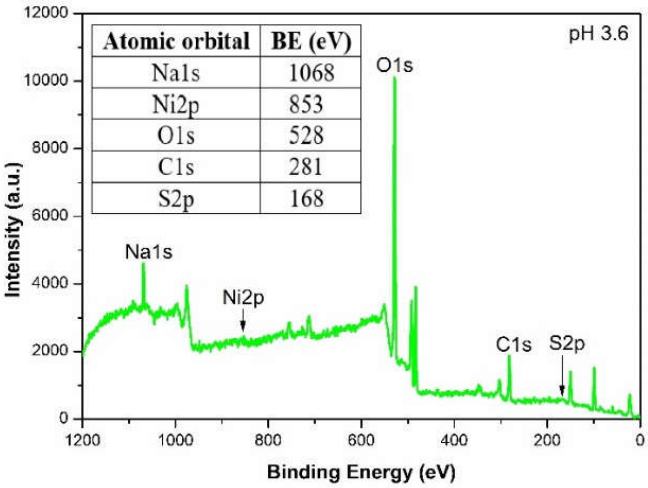
pH 3.6
O1s
Na1s
Ni2p
C1s
S2p
Intensity (a.u.)
Binding Energy (eV)
Atomic orbital | BE (eV)
Na1s | 1068
Ni2p | 853
O1s | 528
C1s | 281
S2p | 168

(c)

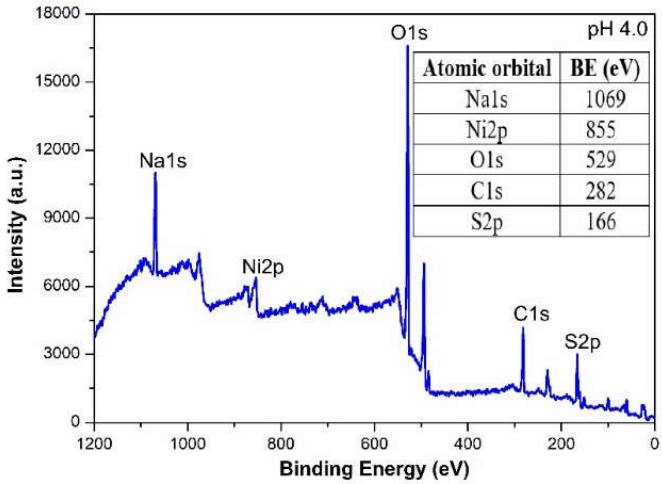

Atomic orbital	BE (eV)
Na1s	1069
Ni2p	855
O1s	529
C1s	282
S2p	166

(d)

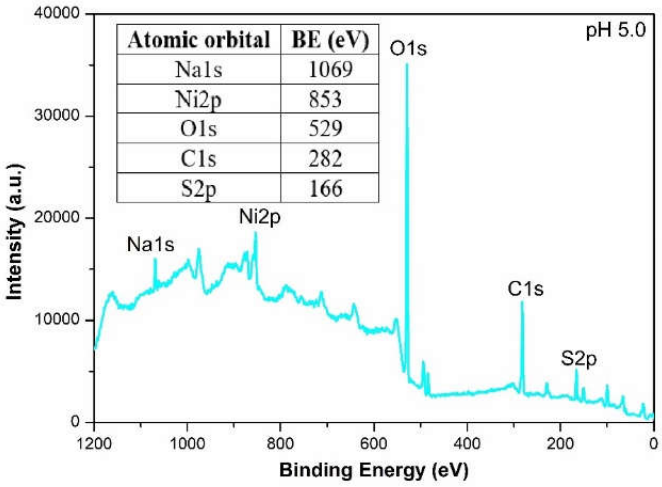

Atomic orbital	BE (eV)
Na1s	1069
Ni2p	853
O1s	529
C1s	282
S2p	166

(e)

Figure 2. XPS studies of nickel sulphide thin films [a] pH 1, [b] pH 2.2, [c] pH 3.6, [d] pH 4, and [e] pH 5.

This finding agreed well with the result obtained from AFM analysis for the film prepared at pH 3.6 as demonstrated in Table 2. Interestingly, the spectra of NiS synthesized at both pH 4 and 5 reveal peaks corresponding to Ni2p and S2p with the Ni^{2+} ions dominating their surfaces (Figure 2d, 2e). Thus pH 4 and pH 5 are found to be the best pH for synthesizing NiS film. However, considering the high intensities of the Ni2p (18,600 a.u.) and S2p (5,163 a.u.) peaks at pH 5.0,

compared to Ni2p (6,375 a.u.) and S2p (3,005 a.u.) peaks at pH 4, it can be concluded that the optimum pH to efficiently synthesize NiS films by chemical deposition is pH 5. This finding is consistent with the results obtained in previous studies [38, 39].

On the other hand, XPS findings confirmed that the nickel sulfide has been successfully deposited on fluorine-doped tin oxide (FTO) substrate under different urea concentrations [40]. Several peaks at 854.1 eV, 871.6 eV, 161.6 eV and 162.7 eV, accounted for $Ni2p_{3/2}$, $Ni2p_{1/2}$, $S2p_{3/2}$, and $S2p_{1/2}$, respectively. Nickel sulfide nanoparticles have been produced using nickel formate and sulfur, in stainless steel autoclave, at 440 °C [41]. In NiS particles, peaks at 853.2 eV & 870.8 eV, and 856.2 eV & 873.8 eV were contributed to $Ni2p_{3/2}$ and $Ni2p_{1/2}$ of Ni(II) and Ni (III) species, respectively. Also, researchers also summarized that bonding energy has moved to 854.5 eV ($Ni2p_{3/2}$) and 872.1 eV ($Ni2p_{1/2}$) in NiS_2 samples because of transfer of coupled electrons. As shown in the XPS data, similar bond energy move could be observed for S2p orbitals, indicating that higher synergistic interaction in NiS_2 particles. It was noted that two peaks have been shifted from 161 eV to 162.8 eV, and 162.1 eV to 164.1 eV, attributed to the $S2p_{3/2}$ and $S2p_{1/2}$, in NiS and NiS_2 samples, respectively.

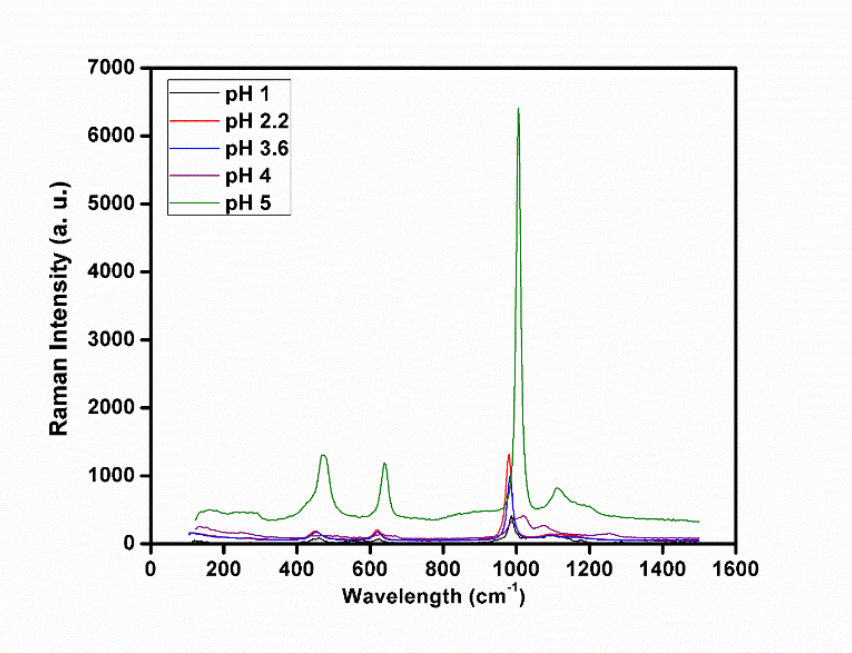

Figure 3. Raman spectroscopy studies of nickel sulfide thin films.

Figure 3 shows the Raman spectra of the NiS thin films prepared at various pH values. Based on the results from the Raman spectroscopic analysis, three peaks located at 456, 622, and 989 cm^{-1} could be seen on the spectra in Figure 3, for the films prepared at all the pH values. These peaks are assigned to the A_{1g} and E_g modes of the NiS films [42]. As the Raman modes of vibration strongly depend on the crystal lattice vibrations, some of the vibration modes of the bulk NiS are not clearly observed due to the reduction in size of the NiS nanostructures [43]. Generally, the Raman study revealed that the formation of the nickel sulfide thin films is strongly dependent on the pH of the solution in the chemical bath. However, it is obviously clear that the intensities of the three peaks at 456, 622, and 989 cm^{-1} for the film prepared at pH 5 are significantly higher compared to those of other pH values. Considering that the intensities of the peaks increase with

increase pH values of the chemical bath solutions, the obtained experimental findings confirmed that the best pH value to efficiently prepare a high-quality thin film of nickel sulfide is pH 5. On the other hand, no sharp features could be observed in 150 cm^{-1} to 400 cm^{-1}, representing that there is no nickel oxide could be identified. Zhe and co-workers [44] also pointed out that their prepared films did not indicate any Raman bands related to the CuO phases. Formation of NiS phase could be confirmed according to Raman spectroscopy results, as reported by AlMalki and co-workers [45]. Raman peaks could be identified at 949, 940, 236, 301, 345, and 533 cm^{-1}, accounted for NiS nanoparticles, prepared using simple hydrothermal method.

CONCLUSION

Various deposition methods have been utilized to produce metal chalcogenide thin films. In this study, nanostructured nickel sulfide thin films were deposited onto microscope glass slides at different pH values, ranging from pH 1 to pH 5 using the chemical bath deposition method. Typically, standard characterization techniques like atomic force microscopy were used to investigate the morphology of fabricated films. In this study, x-ray photoelectron spectroscopy and Raman spectroscopy methods were utilized for the first time. The overall findings verified that high quality films can be obtained in acidic conditions. The Raman spectroscopic analysis revealed that the films produced at pH 4 and pH 5 exhibited smooth, uniform morphology and a homogeneous surface without cracks. In the future, research will focus on power conversion efficiency to verify that the materials developed can be utilized in solar cell applications.

ACKNOWLEDGEMENT

This research work was supported by INTI International University under Research Grant (Seed): INTI-FHLS-12-02-2022.

REFERENCES

1. Nowsherwan, G.; Iqbal, M.; Rehman, S.; Siti, S. Numerical optimization and performance evaluation of ZnPC: PC70BM based dye-sensitized solar cell. *Sci. Rep*. **2023**, 13, 10431.
2. Khmissi, H.; Azeza, B.; Bouzidi, M.; Zainab A. Investigating of an antireflective coating systen for solar cells based on thin film multilayers. *Eng. Technol. Appl. Sci. Res.* **2024**, 14, 14374-14379.
3. Mihai, O.; Schiopu, A.; Marian, V.; Iana, V. Influence of supplementary oxide layer on solar cell performance. *Eng. Technol. Appl. Sci. Res.* **2024**, 14, 13274-13282.
4. Anuar, K.; Ho, S.M.; Saravanan, N.; Atan, S. Influence of complexing agent (Na_2EDTA) on chemical bath deposited Cu_4SnS_4 thin films. *Bull. Chem. Soc. Ethiop*. **2010**, 24, 259-266.
5. Murugesan, N.; Suresh, S.; Kumar, S.; Murugesan, S. Enhancing selectivity of solar absorber using reduced graphene oxide modified nickel oxide nanocomposite thin films. *Sol. Energy* **2022**, 247, 185-195.
6. Vinoth, S.; Ahmed, A.; Santhanam, A. Enhancing the optoelectronic properties of low-cost nebulizer spray pyrolysis (NSP) prepared ZnS thin film through praseodymium doping for photodetector applications. *Mater. Sci. Eng. B*. **2023**, 289, 116213.
7. Chi, Z.; Sartel, C.; Zheng, Y.; Modak, S. Native defects association enabled room-temperature p-type conductivity in β-Ga_2O_3. *J. Alloys Compd.* **2023,** 969, 172454.
8. Hasan, G.; Hazhir, M.; Rostam, M. Effects of deposition time on structural and optical properties of ZnS and ZnS/Au thin films grown by thermal evaporation. *Phys. B Condens. Matter.* **2022**, 627, 413616.

9. Pawan, K.; Rao, G. Comprehensive analysis of microstructural, optical and electrical properties of ZnS thin films deposited by cost effective SILAR technique. *Mater. Today Proc.* **2022***,* 65, 380-384**.**
10. Daniel, A.; Imre, M. Review of photocatalytic ZnO nanomaterials made by atomic layer deposition. *Surf. Interfaces* **2023**, 40, 103094.
11. Sathishkumar, M.; Saroja, M.; Venkatachalam, M. Influence of (Cu, Al) doping concentration on the structural, optical and antimicrobial activity of ZnS thin films prepared by Sol-Gel dip coating techniques. *Optik* **2019**, 182, 774-785.
12. Hao, Z.; Geng, J.; Gao, H.; Hui, X. The development of 3D atomic force microscopy with magnetically driven orthogonal cantilever probes. *Eng*. **2023**, 24, 84-93.
13. Xia, F.; Kamal, Y. Review: Advanced atomic force microscopy modes for biomedical research. *Biosens.* **2022**, 12, 1-24.
14. Anita, D.; Hussain, S.; Nishkala, R.; Mamatha, D. Influence of Bi^{3+} substitution on spin-phonon coupling in $La_{0.7}Sr_{0.3}MnO_3$ Manganites: A Raman spectroscopy study. *Mater. Res. Bull.* **2025**, 186, 113338.
15. Ivan, S.; Azat, A.; Andrey, K.; Pavel. T. Thermal and photochemical degradation of $CsGeI_3$ and $CsGeBr_3$: XPS and optical studies. *Opt. Mater.* **2024**, 157, 116303-116303.
16. Huo, J.; Wu, J.; Min, Z.; Tu, Y. Effect of ammonia on electrodeposition of cobalt sulfide and nickel sulfide counter electrodes for dye-sensitized solar cells. *Electrochim. Acta* **2015**, 180, 574-580.
17. Momeni, M.; Ghayeb, Y.; Akbarnia, M. Successive ionic layer adsorption and reaction (SILAR) deposition of nickel sulfide on the Fe_2O_3 nanotube for efficient photocathodic protection of stainless steel under visible light. *J. Iran. Chem. Soc.* **2020**, 17, 3367-3374.
18. Karthik, R.; Malik, A.; Paul, O.; James, R. Nickel sulfide thin films from thio- and dithiobiuret precursors. *Chem. Mater.* **2010**, 22, 6328-6340.
19. Yasmin, F.; Saddam, M.; Bhuiyan, H.; Jellur, R. A comprehensive study on structural and optical properties of zinc selenide/poly ortho-methoxyaniline hybrid thin films deposited by chemical bath deposition and plasma polymerization techniques. *Arab. J. Chem.* **2024**, 17, 105842.
20. Nauman, K.; Athar, J.; Bashir, M.; Shazia, B. Role of triethanolamine complexing agent in chemical bath deposition of tin sulfide thin films: Microstructural and optical properties. *Results Opt.* **2024**, 14, 100610.
21. Rehman, A.; Ali, A.; Ikram, S.; Mahmood, K. Emerging pathways in thermoelectric: Chemical bath deposition of magnesium selenide thin films for sustainable energy harvesting. *Ceram. Int.* **2024,** 50, 20758-20763.
22. Arsad, A.; Zuhdi, A.; Arzaee, A.; Harif, M. Effects of post-deposition treatment on zinc sulfide thin films prepared by an effective-cost chemical bath deposition method. *Ceram. Int.* **2024**, 50, 18697-18707.
23. Junaid, Y.; Warda, S.; Ismail, B.; Fazal, T. Engineering the optical properties of nickel sulphide thin films by zinc integration for photovoltaic applications. *RSC Adv.* **2023**, 13, 27415-27422.
24. Sartale, S.; Lokhande, D. Growth of copper sulphide thin films by successive ionic layer adsorption and reaction (SILAR) method. *Mater. Chem. Phys.* **2000**, 65, 63-67.
25. Tun, M.; Pansa, P.; Ruankham, P. Improving morphology and optoelectronic properties of ultra-wide bandgap perovskite via Cs tuning for clear solar cell and UV detection applications. *Sci. Rep.* **2023**, 13, 1-12.
26. Murugesan, R.; Sivakumar, S.; Karthik, K. Structural, optical and magnetic behaviors of Fe/Mn-doped and co-doped CdS thin films prepared by spray pyrolysis method. *Appl. Phys. A* **2019**, 125, 1-13.
27. Sivakumar, S.; Karthik, K.; Haris, M. Effect of Mg/Co on the properties of CdS thin films deposited by spray pyrolysis technique. *Curr. Appl. Phys*. **2019**, 19, 1136-1144.

28. Pakiyaraj, K.; Kirthika, V.; Karthik, K. Effect of annealing on the structural, morphological, optical and electrical properties of Al-Zn co-doped SnO_2 thin films. *Mater. Res. Innov.* **2020**, 24, 193-201.
29. Gahtar, A.; Sayah, A.; Boukacham, A.; Zaouche, C. Effect of temperature on the properties of nickel sulfide films performed by spray pyrolysis technique. *Adv. Mater. Sci.* **2020**, 20, 36-51.
30. Rekha, B.; Jha, R.; Medha, B.; Reetu, S. Electrochemical studies of synthesized nickel sulphide nanoparticles. *Mater. Today Proc.* **2022**, 48, 658-660.
31. Muthu, S.; Gopalan, M. Mesoporous nickel sulphide nanostructures for enhanced supercapacitor performance. *Appl. Surf. Sci.* **2019**, 480, 186-198.
32. Arulkumar, E.; Rajkumar, S.; Wasihun, W.; Thanikaikarasan, S. Influence of solution pH dependency on structure, optical with photo electrochemical characteristics of SILAR deposited copper oxide thin films. *Heliyon* **2024**, 10, e33579.
33. Kariper, A.; Guneri, E.; Gode, F.; Gumus, C. Effect of pH on the physical properties of CdS thin films deposited by CBD. *Chalcogenide Lett.* **2012**, 9, 27-40.
34. Balayeva, O.; Azizov, A.; Mustafa, B.; Rashid, J. Effect of thermal annealing on the properties of nickel sulfide nanostructures: Structural phase transition. *Mater. Sci. Semicond. Proc.* **2017,** 64, 130-136.
35. Zhang, A.; Li, W.; Zhang, Z.; He, J.; Ning, X. NiS_2@ MWCNTs as a promising anode material for lithium and sodium-ion batteries with superior cycling stability. *J. Alloys Compd*. **2024**, 971, 172669.
36. Gao, Z.; Chen, C.; Chang, J.; Chen, L. Porous Co_3S_4@ Ni_3S_4 heterostructure arrays electrode with vertical electrons and ions channels for efficient hybrid supercapacitor. *Chem. Eng. J.* **2018**, 343, 572-582.
37. Murthy, A.; Theerthagiri, J.; Madhavan, J.; Murugan, K. Electrodeposited carbon-supported nickel sulfide thin films with enhanced stability in acid medium as hydrogen evolution reaction electrocatalyst. *J. Solid State Electrochem.* **2018**, 22, 365-374.
38. Jeong, Y.; Manthiram, A. Synthesis of nickel sulfides in aqueous solutions using sodium dithionite. *Inorg. Chem.* **2001**, 40, 73-77.
39. Hu, Q.; Zhang, S.; Li, W.; Xiong, J. Regulating the structure and morphology of nickel sulfides for electrochemical energy storage: the role of solvent pH. *Chem. Eng. J.* **2022**, 441, 136130.
40. Venkata, M.; Chandu, V.; Kim, S.; Lee, J. Solution-processed morphology-controllable nanosphere structured highly efficient and stable nickel sulfide counter electrodes for dye- and quantum dot-sensitized solar cells. *New J. Chem.* **2015**, 39, 9575-9585.
41. Jiwei, Z.; Zhang, D.; Wang, Y.; Wang, S. Targeted synthesis of NiS and NiS_2 nanoparticles for high−performance hybrid supercapacitor *via* a facile green solid−phase synthesis route. *J. Energy Storage* **2020**, 32, 101852.
42. Krishnamoorthy, D.; Prakasam, A. Low-cost and novel preparation of porous NiS_2/graphene heterojunctions photoanodes for high-efficiency dye-sensitized solar cells. *Inorg. Chem. Commun.* **2020**, 119, 1-18.
43. Trishala, R.; Desai, R.; Prasad, G.; Tukaram, D. Evaluation of nanostructured NiS_2 thin films from a single-source precursor for flexible memristive devices. *ACS Omega* **2023**, 8, 48873-48883.
44. Cheng, Z.; Harry, A.; Liu, M. Raman Spectroscopy of Nickel Sulfide Ni_3S_2. *J. Phys. Chem. C* **2007**, 111, 17997-18000.
45. AlMalki, M.; Ziya, K.; Waleed, A. Synthesis and characterization of Nickel sulfide and Nickel sulfide/ Molybdenum disulfide nanocomposite modified ITO electrode as efficient anode for methanol electrooxidation. *Appl. Surf. Sci. Adv.* **2021**, 6, 100187.